High-pressure phase transition in brucite, Mg(OH)$_2$

Thomas S. Duffy, Charles Meade, Yingwei Fei, Ho-Kwang Mao, Russell J. Hemley

Geophysical Laboratory and Center for High-Pressure Research, Carnegie Institution of Washington,
5251 Broad Branch Road NW, Washington, DC 20015, U.S.A.

Abstract

Brucite, Mg(OH)$_2$, was investigated by Raman spectroscopy to pressures of 36.6 GPa under nonhydrostatic conditions and to 19.7 GPa under quasi-hydrostatic conditions. Several new Raman lines are first observed at 4 GPa, demonstrating the existence of a high-pressure structural change. One of the new lines grows over a broad pressure interval, and this growth can be explained by a resonant interaction with the E$_g$ translational mode. Raman data are compared with recent infrared spectroscopy, X-ray diffraction, and neutron diffraction studies of brucite. The structural change is likely to involve displacement or disordering of the H atoms, consistent with neutron diffraction results. The Raman-active O-H stretching vibration in brucite decreases with pressure at the rate of ~7 cm^{-1}/GPa, larger than the pressure dependence of the infrared-active stretching vibration by more than a factor of ten. The primary differences in the Raman spectra of Mg(OH)$_2$ and Ca(OH)$_2$ are that the O-H vibrational frequencies in Mg(OH)$_2$ vary linearly with pressure, and the O-H stretching vibration band width increases with pressure at a rate that is an order of magnitude lower for Mg(OH)$_2$ than for Ca(OH)$_2$.

Introduction

The high-pressure behavior of brucite, Mg(OH)$_2$, is of considerable interest for studying such diverse phenomena as dehydration reactions at high pressure, compression-induced amorphization, and the behavior of hydrous minerals in the Earth's upper mantle. The discovery of large numbers of magnesian silicates containing structurally bound OH (Finger and Prewitt, 1989; Kanzaki, 1991) has raised questions concerning the potential role of such phases in the Earth's interior. Because of its structural and chemical simplicity, brucite serves as a useful prototype for hydrous and layered minerals at high pressures. Thermodynamic properties of brucite have been investigated in several recent studies. The equation of state has been measured under shock compression (Simakov et al., 1974; Duffy et al., 1991) and under high static pressures (Fei and Mao, 1993; Catti et al., 1995; Duffy et al., 1995). Measurements of the thermal expansivity at both ambient and high pressure have also been reported (Redfern and Wood, 1992; Fei and Mao, 1993). Neutron diffraction has been conducted at elevated pressures on both normal (Catti et al., 1995) and deuterated samples (Parise et al., 1994). The structure and bonding of Mg(OH)$_2$ has been investigated theoretically using the Hartree-Fock approximation (Sherman, 1991; D'Arco et al., 1993).

The phase equilibria of brucite have been the subject of high-pressure experimental investigations from the 1940s to the present. Such studies (e.g., Bowen and Tuttle, 1949; Kennedy, 1956; Irving et al., 1977) have fo-cused on determining the brucite-periclase dehydration curve, which also constrains the thermodynamic properties of H$_2$O under conditions of the lower crust and mantle. Advances in multi-anvil press technology have recently enabled the dehydration reaction to be studied up to 15 GPa and 1500 K (Leinenweber et al., 1993; Johnson and Walker, 1993). Detailed analyses of the results require accurate characterization of the thermodynamic properties of brucite.

Pressure-induced amorphization has now been documented in many materials. Portlandite, Ca(OH)$_2$, which is isomorphous with brucite, amorphizes when compressed above 11 GPa at room temperature (Meade and Jeanloz, 1990). In addition to the loss of X-ray diffraction peaks, significant changes in the Raman and infrared spectra of this material have been observed (Kruger et al., 1989; Meade et al., 1992; Duffy, in preparation). In contrast, brucite has been found to be stable to 78 GPa by X-ray diffraction (Fei and Mao, 1993) and to 34 GPa by infrared spectroscopy (Kruger et al., 1989). As appears to be the general case for materials undergoing these transitions, the amorphization of Ca(OH)$_2$ has been interpreted as the result of a frustrated phase transition. However, no such phase transition in brucite has been detected by shock compression, static compression, or infrared spectroscopy experiments over a broad pressure and temperature range.

Brucite crystallizes in the trigonal CdI$_2$ structure ($P\bar{3}m1$) (Bernal and Megaw, 1935; Petch and Megaw, 1954; Elleman and Williams, 1956; Zigan and Rothbauer, 1967). This is a layered structure in which each Mg ion is sur-
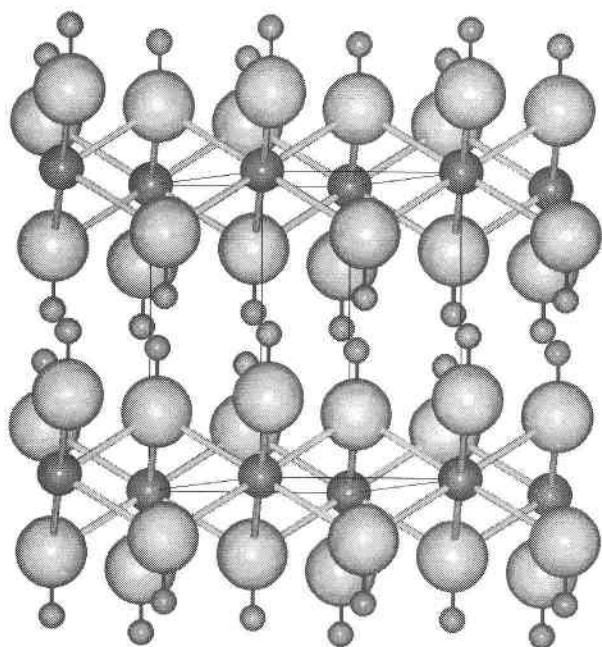
Fig. 1. Crystal structure of brucite. The large spheres are O atoms, the intermediate spheres are Mg atoms, and the small spheres are H atoms. The O-H bonds are directed along the c axis.

TABLE 1. Pressure dependence of the Raman modes of brucite

Mode	ν_0^* (cm^{-1})	$\partial\nu/\partial P^*$ (cm^{-1}/GPa)	ν_0^{**} (cm^{-1})
$E_g(T)$	280.0	$5.40 - 0.15P$	280
	359.6	$0.60 + 0.04P$	
	383.8	2.18	
	408.1	$4.21 - 0.20P$	
$A_{1g}(T)$	444.7	$6.93 - 0.15P$	443
$E_g(R)$	727.5	—	725
$A_{1g}(I)$	3652.0	-7.68	3652
	3661.3	-5.34	

* Data from this study.
** Data from Dawson et al. (1973).

EXPERIMENTAL TECHNIQUE

Brucite was synthesized in a piston-cylinder apparatus at 1.5 GPa and 1073 K under H_2O-saturated conditions. The samples were produced in the same experiment as those used in high-pressure X-ray diffraction studies (Fei and Mao, 1993; Duffy et al., 1995). The crystals were transparent platelets with lateral dimensions up to 50 μm and thicknesses of <10 μm. Ambient-pressure Raman spectra and X-ray diffraction confirmed that the samples were brucite and no impurity phases were detectable.

Raman experiments were carried out in a Mao-Bell diamond-anvil cell with 600-μm culet type I diamonds. The sample was loaded into a hole 300 μm in diameter and 75 μm thick in a T301 steel gasket. Brucite samples were compressed both nonhydrostatically (with no pressure medium) and under quasi-hydrostatic conditions using Ne as a pressure medium. Raman spectra were recorded with a multichannel Raman microprobe (Dilor XY) in a backscattering configuration using a charge-coupled device (CCD) detector with 1024×298 channels (e.g., Hemley, 1987). The excitation source was Ar$^+$ laser operated at either 488.0 or 514.5 nm at powers of 100 mW or less. The laser light was focused onto the sample and Raman signal collected using a Leitz L25 objective. Data accumulation times ranged from 100 to 3000 s. Peak positions and widths were determined by fitting the spectra to Lorentzian line shapes with background subtraction.

Pressures were determined from the fluorescence of small ruby chips (1–5 μm) distributed through the sample volume (Mao et al., 1986). Pressure was measured both before and after collecting Raman spectra at several positions within the chamber. In experiments with no pressure medium, the R_1 and R_2 ruby fluorescence peaks were not always well resolved, and pressure differences of ~1 GPa could develop across the sample chamber. For the Ne medium experiments, the pressure varied by <0.1 GPa across the sample, and the two ruby fluorescence peaks were always well resolved. For decompression experiments, the pressure before and after taking Raman measurements varied by up to 2.5 GPa.

RESULTS

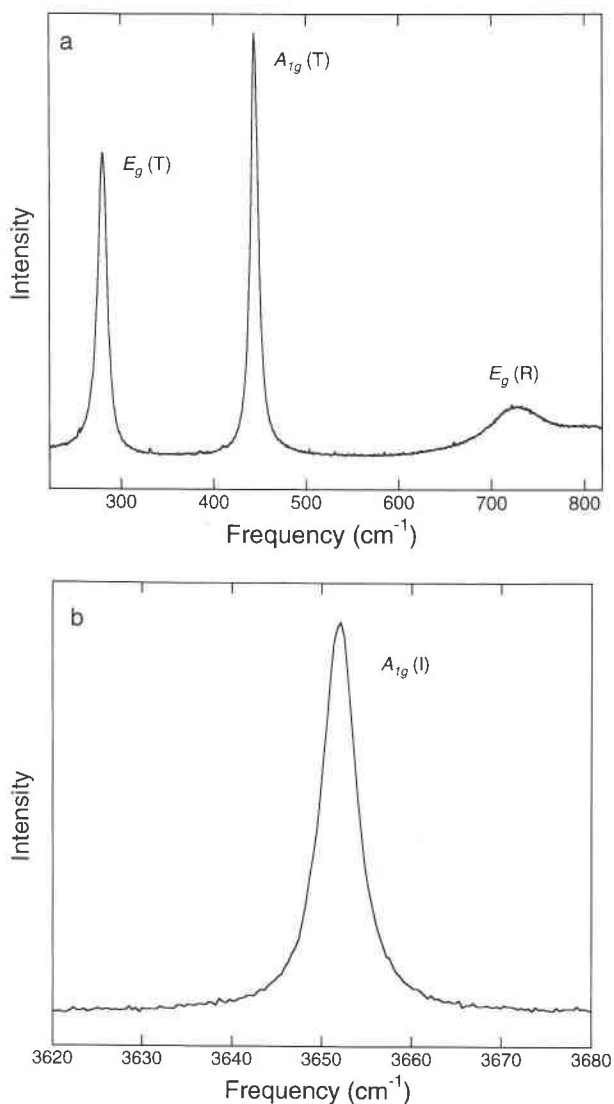Ambient-pressure Raman spectra for brucite are shown in Figure 2 and Table 1. All four Raman active modes of

rounded by a distorted octahedron of O atoms (Fig. 1). The Mg ions lie in planes with the O ions above and below them in a sandwich arrangement. The O-H bonds are perpendicular to these planes. The brucite layers are stacked along the c direction and held together by weak interlayer forces. There is conflicting evidence regarding the nature of these forces. On the basis of the interlayer O distances, Bernal and Megaw (1935) concluded the layers were held together by weak dipole forces. X-ray emission spectra, however, support the existence of some H bonding between the layers (Haycock et al., 1978). Ab initio Hartree-Fock studies, however, have failed to find evidence for H bonding at ambient or elevated pressure (Sherman, 1991; D'Arco et al., 1993).

Factor group analysis indicates there are six allowed lattice modes for brucite: three of these are infrared active, and three are Raman active (Mitra, 1962). In addition, there are Raman- and infrared-active internal modes. The lattice vibrations consist of translational modes that correspond to vibrations of the O-H units that are either parallel [$A_{1g}(T)$ and $A_{2u}(T)$] or perpendicular [$E_g(T)$ and $E_u(T)$] to the c axis. There are also rotational vibrations of the OH ions: $E_g(R)$ and $E_u(R)$. The internal modes are symmetric (Raman-active) and antisymmetric (infrared-active) O-H stretching vibrations [$A_{1g}(I)$ and $A_{2u}(I)$]. Ambient-pressure polarized Raman and infrared spectra (Dawson et al., 1973) from normal and deuterated samples have been used to make mode assignments (Table 1).

Fig. 2. Ambient-pressure Raman spectra of brucite. The external modes are shown in **a**, and the O-H stretch vibration is shown in **b**.

Fig. 3. Raman spectra of brucite under quasi-hydrostatic conditions. (**a**) External modes, (**b**) internal modes. The pressure (in GPa) is listed next to each trace. New peaks in the Raman spectrum can be observed between 350 and 450 cm^{-1} in **a** and on the high-frequency side of the O-H fundamental in **b**. The background diamond fluorescence in **a** is shown as the bottom trace.

brucite were detected, and the agreement with previous data (Dawson et al., 1973) is excellent. We confirmed assignments of the rotatory and translatory modes by making additional measurements on deuterated samples. Our results for $Mg(OD)_2$ are also in good agreement with the data of Dawson et al. (1973). The $E_g(R)$ mode for both $Mg(OH)_2$ and $Mg(OD)_2$ is very broad, possibly exhibiting multiphoton structure.

A large number of Raman spectra were recorded under both increasing and decreasing pressure under both quasi-hydrostatic and nonhydrostatic conditions. Representative spectra for the quasi-hydrostatic experiments are shown in Figures 3 and 4. The peak pressures achieved were 19.7 GPa under quasi-hydrostatic conditions and 36.6 GPa under nonhydrostatic conditions. Three of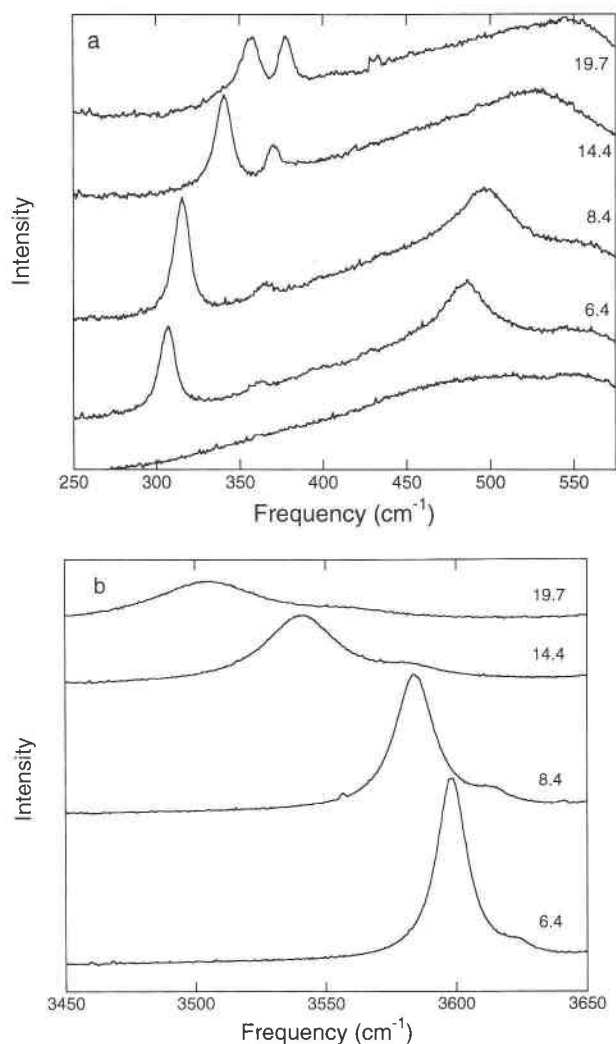 the four brucite Raman peaks were detected at elevated pressures. The $E_g(R)$ peak was not detected because of its low intensity and its location in a region of strong diamond fluorescence.

The Raman spectra of brucite exhibit a number of unexpected features at high pressures. The most significant observation is the appearance of a new line on the high frequency side of the $E_g(T)$ mode (Fig. 3a). In the nonhydrostatic experiments, the peak was first detected at 14.3 GPa (Duffy et al., 1993). Below this pressure, the low signal to noise ratio of these experiments prevented observation of this peak. This conclusion was subsequently verified by recording a higher quality spectrum under nonhydrostatic conditions at 7.3 GPa, which clearly showed the existence of a weak additional peak at 368

cm^{-1}. The evolution of the new peak is similar under both quasi-hydrostatic and nonhydrostatic conditions. The $E_g(T)$ peak decreases in amplitude, and the new peak increases such that they are of roughly equal intensity near 20 GPa (Fig. 3a). At higher pressures this behavior continues, and at 36.6 GPa the new peak has an amplitude 6.5 times larger than that of the E_g peak. The other lattice vibration, A_{1g}, becomes weak and broad at high pressure and is barely detectable above 20 GPa.

A shoulder (at 3624 cm^{-1}) on the high-frequency side of the O-H stretching vibration is also evident in the quasi-hydrostatic experiments (Fig. 3b). This peak persists to the highest pressures without appreciable change in intensity. In the nonhydrostatic experiments, this peak is only detectable in few spectra, again owing to the lower signal to noise ratio of those experiments. The O-H stretching vibration also weakens and broadens at high pressures.

Additional quasi-hydrostatic Raman spectra were obtained between 1 and 10 GPa to characterize the observed changes better (Fig. 4). These spectra were obtained by first raising the pressure to 6 GPa and then adjusting the pressure both upward and downward. All changes to the spectra appear to be reversible in this pressure range. In the low-frequency region (Fig. 4a), three weak new peaks were observed between the A_{1g} and E_g modes. The peak near 360 cm^{-1} increases in intensity with pressure (Fig. 3a), but the other two modes remain weak. The mode near 410 cm^{-1} is evident at pressures as low as 1.1 GPa, whereas the other two modes are first detectable at 4.4 GPa. Similarly, the high-frequency shoulder on the O-H stretch vibration first appears at 4.4 GPa (Fig. 4b).

The quasi-hydrostatic and nonhydrostatic brucite spectra show qualitatively similar behavior. The frequencies of the lattice vibrations increase with pressure, whereas the O-H stretch exhibits a negative frequency shift. The latter is consistent with infrared data (Kruger et al., 1989). The A_{1g} modes, both internal and external, become broad and weak at high pressures. The pressure dependences of the frequencies and the full widths at half maximum (FWHM) are shown in Figures 5 and 6.

For the lattice vibrations, the pressure dependence of the frequency shifts is nearly the same under both quasi-hydrostatic and nonhydrostatic conditions (Fig. 5a). The frequencies and their pressure derivatives are listed in Table 1. Upon decompression, the behavior is reversible, although the measured frequencies tend to lie slightly below their values upon compression. When decompressed from high pressure ($\geq$20 GPa), the peak amplitudes are much reduced until near ambient pressure ($\sim$2 GPa), at which point the intensities suddenly recover. For the O-H stretch vibration (Fig. 5b), the pressure dependence of the mode is slightly greater in the quasi-hydrostatic experiment (-7.7 cm^{-1}/GPa) than in the nonhydrostatic experiment (-6.7 cm^{-1}/GPa). The peaks returned to their original positions at ambient pressure, but some residual broadening is evident.
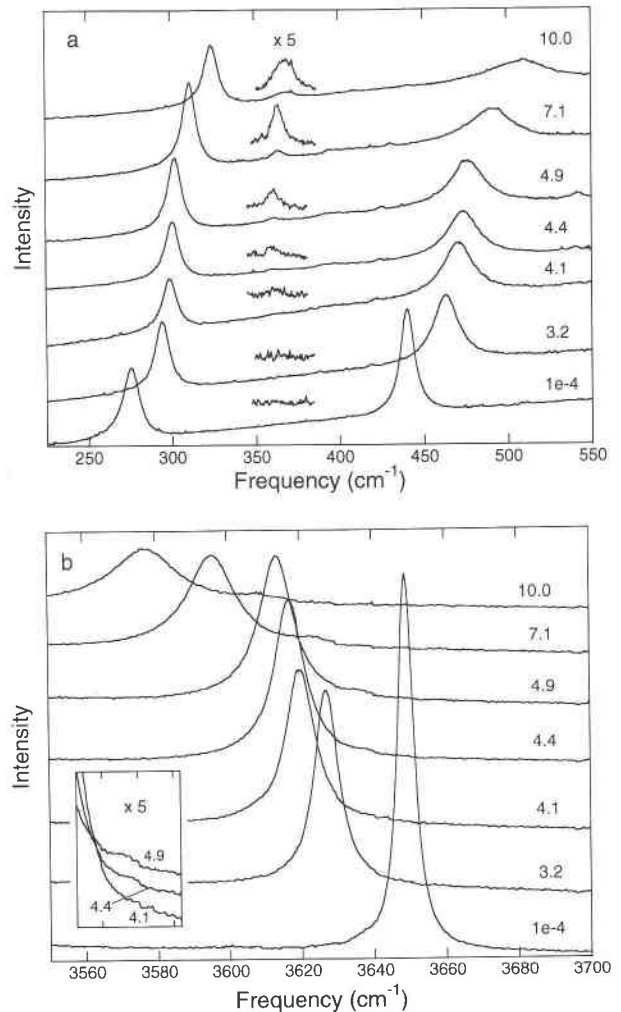

Fig. 4. Raman spectra of brucite under quasi-hydrostatic conditions to 10 GPa. (a) External modes, (b) internal modes. New Raman peaks are observable beginning at 4.4 GPa. An expanded version of the 360-cm^{-1} region is shown above each trace in **a**. The inset in **b** shows the appearance of the high-frequency sideband at 4.4 GPa.

The lattice and O-H stretch vibrations also display contrasting behavior with regard to band widths. For the lattice vibrations, the pressure dependence of the FWHM is similar under both quasi-hydrostatic and nonhydrostatic conditions (Fig. 6a). This indicates that the broadening observed for the A_{1g} peak is intrinsic and cannot be attributed to pressure gradients. The E_g lattice vibration and the 360-cm^{-1} mode display little change in FWHM with pressure. The FWHM of the O-H stretch vibration broadens with pressure at a rate comparable with the lattice A_{1g} mode (Fig. 6b). However, in this case there is a significant difference in band width between the quasi-hydrostatic and nonhydrostatic experiments. Nevertheless, it appears that this broadening is largely intrinsic, and only a portion is due to nonhydrostatic pressure distribution. The broadening of the band width for the O-H
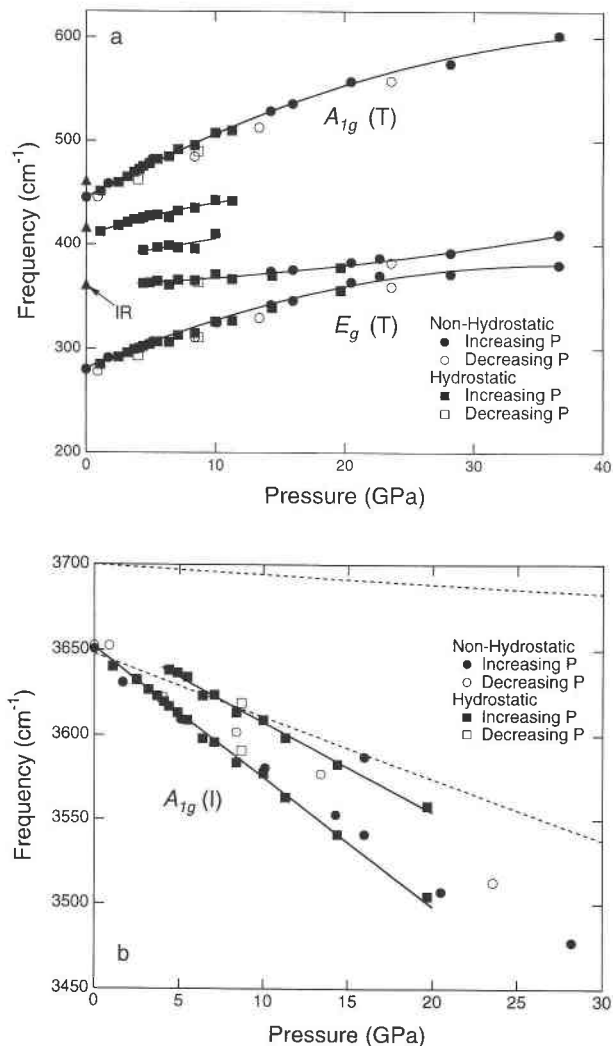
Fig. 5. Pressure dependence of (a) the lattice vibrational frequencies and (b) the O-H stretching frequencies. Triangles at ambient pressure show frequencies of infrared fundamental modes. The upper and lower dashed lines in **b** show the pressure dependence of the fundamental infrared O-H vibrational frequency and the overtone as determined by Kruger et al. (1989).

stretch vibration under nonhydrostatic conditions is similar to that observed for the infrared active vibration (~3 cm^{-1}/GPa) (Kruger et al., 1989). The increased width was attributed to increased anharmonic behavior in that study.

DISCUSSION

Phase transition

The new bands in the Raman spectrum of brucite indicate that there is a pressure-induced structural change (Fig. 4). One of the new peaks subsequently grows in intensity over a broad pressure interval, while the others remain weak or disappear. The appearance of a weak new peak near 410 cm^{-1}, observed at pressures as low as 1.1 GPa, suggests the possibility of an additional transition.
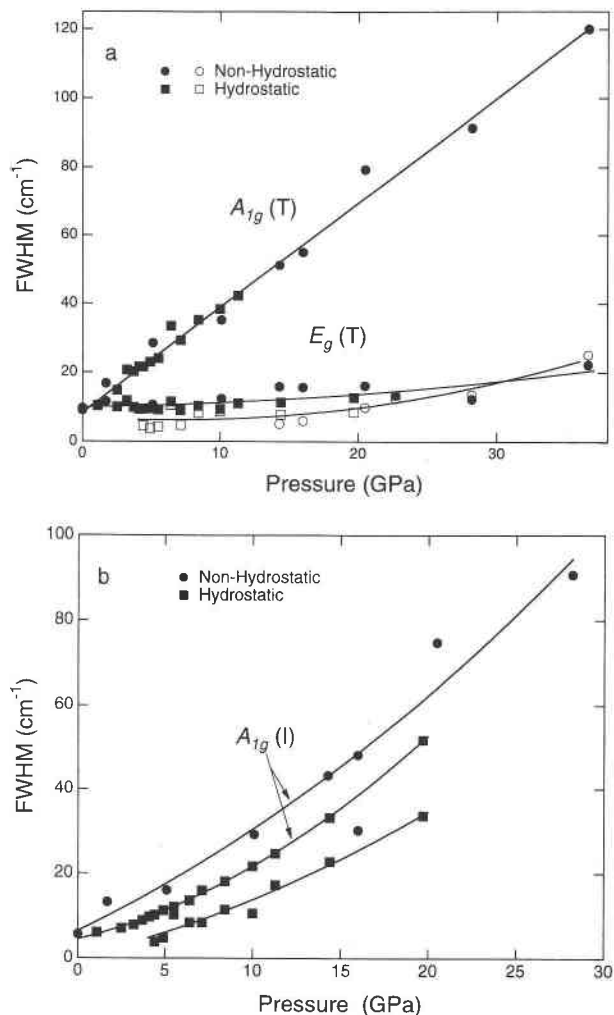

Fig. 6. Full width at half-maximum (FWHM) for (a) the lattice vibrational modes and (b) the O-H stretch vibrations. Open symbols in **a** are for the 360-cm^{-1} peak.

This feature remains weak in subsequent spectra. The spectra shown in Figure 4 were not measured as a function of increasing pressure, but the pressure was cycled up and down to identify the lowest pressure at which phase transition features could be detected. The weak band observed at 1.1 GPa may represent an irreversible effect of the transition first detected at 4 GPa. The other new peaks disappear below 4 GPa, however.

Extrapolating the peak at 1.1 GPa to ambient pressure yields a frequency of 408 cm^{-1} (Table 1). There is a strong A$_{1g}$ line of ruby found at 417 cm^{-1} at ambient pressure; however, this assignment is ruled out because the band is also observed in samples with no ruby present. The peak lies near the frequency of the E$_u$(R) infrared-active mode at 416 cm^{-1} (Dawson et al., 1973). Similarly, the new peak near the E$_g$(T) mode extrapolates to 360 cm^{-1} at ambient pressure, close to the E$_u$(T) infrared-active mode at 361 cm^{-1}. Thus, two of the three new Raman lattice vibrations correspond closely to frequencies of in-

frared fundamental modes. Infrared fundamental modes also occur at 461 and 3688 cm^{-1} (Dawson et al., 1973).

A phase transition in brucite is surprising in that no evidence for such a transition was found in previous X-ray diffraction, shock compression, and infrared spectroscopy experiments. A detailed comparison with previous data, however, shows that there are significant changes in the structural response of the material at high pressure. Furthermore, more recent neutron diffraction data provide support for a high-pressure structural change in this material (Parise et al., 1994; Catti et al., 1995).

Fermi resonance

The appearance of new bands in the Raman spectrum of brucite suggests either a reduction of symmetry or an increase in the number of atoms in the unit cell. The appearance of two new lattice modes close to fundamental infrared frequencies suggests a mixing of formerly pure infrared and Raman modes. The subsequent growth of the 360-cm^{-1} peak can be explained in one of two ways. One possibility is that the transformation occurs over a broad mixed-phase region. This does not explain why there is no similar growth in the other new modes, however.

A second possibility is that the peak grows by means of a resonant interaction with the E_g mode initially at 280 cm^{-1}. A Fermi resonance occurs when energy levels of two vibrations of the same symmetry are nearly degenerate. Anharmonic coupling of the two vibrational states shifts the energy levels of both vibrations and leads to an intensity transfer from the strong band to the weaker band. Pressure tuning of Fermi resonances have been documented in a number of molecular crystals (Lewis and Sherman, 1979; Shimizu, 1985; Bier and Jodl, 1987; Olijnyk et al., 1988; Kawai et al., 1990). The behavior of the low-frequency modes of brucite display the characteristics of a resonant interaction: (1) the modes approach each other, reach a minimum in their frequency separation, and move away from each other at higher pressure; (2) the intensity shifts from one mode to the other with increasing pressure, and the intensities are approximately equal at the point of closest approach; and (3) the band width of the initially weak mode becomes larger than that of the initially strong mode at the crossover point. If the 360 cm^{-1} mode corresponds to the E_u fundamental, the modes have the same symmetry, as required for the interaction.

The half-separation between the observed mode frequencies (ν_+ and ν_-) is shown in Figure 7a. A minimum
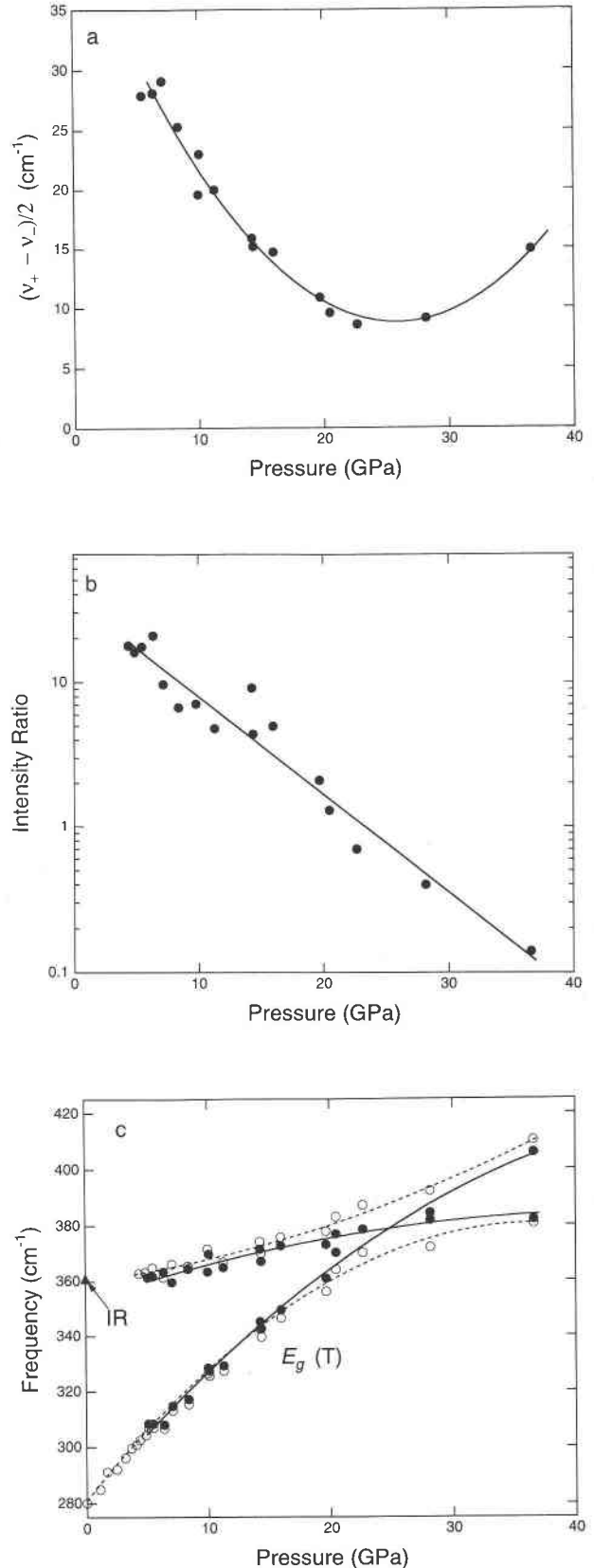

Fig. 7. (a) Half-separation of observed frequencies of the resonant modes as a function of pressure. (b) Intensity ratio of ν_- and ν_+ peaks with pressure. (c) Pressure dependence of the observed Fermi doublet (open symbols) and calculated frequencies without interaction (solid symbols). Dashed lines show measured pressure dependences of the mixed modes, and solid curves show calculated trends for the unperturbed frequencies.

separation of approximately 9 cm^{-1} is reached at ~24 GPa. The ratio of the integrated areas of the two peaks is shown in Figure 7b. The pressure dependence of the intensity ratio is approximately exponential, as expected for a resonant interaction (Hanson and Jones, 1981; Shimizu, 1985). Perturbation theory (Sushchinskii, 1972) can be used to determine the positions of the peaks in the absence of the resonance. The relationship between the perturbed (ν_+ and ν_-) and unperturbed (ν_a and ν_b) frequencies is given by

$$(\nu_+ - \nu_-)^2 = (\nu_a - \nu_b)^2 + 4\delta^2 \qquad (1)$$

where δ is a coupling constant that is assumed to be pressure independent and is given by the minimum value of the half-separation (Fig. 7a) (Lewis and Sherman, 1979). The unperturbed frequencies obtained by solving Equation 1 for ν_a and ν_b are shown as a function of pressure in Figure 7c. The pressure dependence of the unperturbed E_g mode is given by $\nu = 280 + 5.16P - 0.05P^2$.

From Figure 7 it is clear that the observed behavior of the two low-frequency modes of brucite is consistent with a resonant interaction. This is the first time such an interaction has been documented in a hydroxide. The present case is also unusual in the very broad pressure interval over which the interaction is observed. The magnitude of the coupling coefficient ($\delta \sim 9$ cm^{-1}) is much smaller here than in the classic Fermi resonance of solid CO_2 ($\delta \sim 50$ cm^{-1}).

Comparison with infrared spectra

Kruger et al. (1989) reported infrared vibrational spectra for brucite and portlandite to 34 and 24 GPa, respectively. A comparison of the pressure dependence of the infrared and Raman O-H stretching frequencies for brucite is shown in Figure 5b. The pressure dependence of the Raman fundamental vibration (approximately 7 cm^{-1}/GPa) is an order of magnitude larger than that of the infrared fundamental vibration (−0.6 cm^{-1}/GPa). Kruger et al. (1989) attributed the negative frequency shift to increased H bond strength at high pressure. Specifically, interlayer compression increases the strength of the bonding between the H and the O atoms in the next layer. This decreases the attractive force between the intralayer O and the H, and the decrease in O-H oscillation frequency reflects lengthening of the O-H bond. However, neutron diffraction data for brucite indicate that O-H bond distances may remain nearly constant with pressure (Catti et al., 1995), and decreases in the O-H stretch frequency may instead reflect changes in the O-H potential with pressure, as has been proposed to explain similar results for deuterated ice VIII (Nelmes et al., 1993). As discussed below, neutron diffraction data are consistent with disordering of H positions at high pressure, which implies increased interlayer interaction and enhanced H bonding at high pressure. The assumption that the O-H distance increases as O···O decreases needs to be carefully examined, however. In an ab initio Hartree-Fock study (Sherman, 1991), no evidence for enhanced H

bonding was found at high pressure. The possibility of changes in the H positions was not considered in that study.

The infrared absorption spectrum of brucite is complex in the region between 3000 and 4400 cm^{-1} and includes numerous combination bands (Dawson et al., 1973). Kruger et al. (1989) observed a band at 3648 cm^{-1}, which they identified as a hot band caused by the transition of the first excited state to the first overtone. The frequency and the pressure dependence of this band are similar to those of the peak we observed on the high-frequency side of the A_{1g} mode, although slightly different pressure dependences are evident. This similarity also suggests a common origin for the two bands; this could arise from a mixing of formally infrared and Raman modes due to structural distortion or disorder. This band is not observed in the ambient-pressure Raman spectrum of brucite (Fig. 2b) or below 4.4 (Fig. 4b). The Raman and infrared results for the fundamental O-H stretching vibrations display similar broadening and weakening of the peaks with increasing pressure.

X-ray and neutron diffraction

X-ray diffraction of brucite using synchrotron radiation was carried out by Fei and Mao (1993) to 78 GPa and 600 K. More recently, powder diffraction experiments have been carried out by Catti et al. (1995) to 10 GPa and single-crystal diffraction experiments to 14 GPa using synchrotron radiation (Duffy et al., 1995). No direct evidence for a high-pressure phase change was found over the pressure range of these experiments in that neither new X-ray diffraction lines nor any volume discontinuity was detected. Thus, there appears to be no fundamental change to the underlying Mg-O sublattice. This rules out, for example, the possibility that brucite is transforming to a related structure, such as the $CdCl_2$ structure. Materials that crystallize in the CdI_2 structure often form numerous polytypes. Existing X-ray and neutron diffraction data, however, show no evidence for the superlattice reflections that would be expected in this case. Since the X-ray diffraction data are only weakly sensitive to the positions of the H atoms, we suggest that a transition largely involving rearrangements of the H atoms could be consistent with both the Raman and X-ray diffraction data.

X-ray studies of brucite reveal that significant changes in the compression mechanism occur at pressures corresponding to those over which the changes in the Raman spectrum are observed. The pressure dependence of the axial c/a ratio changes dramatically with pressure (Fig. 8). At low pressures, this ratio decreases rapidly from 1.51 at ambient pressure (and 300 K) to values near 1.43 at 11 GPa. Above 8 GPa, the ratio is constant or increases slightly. The unusual behavior of the c/a ratio reflects a change in the relative compressibility of the material along the two directions. Initially, the c-axis compressibility is approximately 5 times larger than the a-axis compressibility (Fei and Mao, 1993). The compressibility

along **c** decreases rapidly with pressure until the compressibilities are nearly equal above 8 GPa.

The large decrease in the compressibility of brucite along the **c** direction reflects structural changes in the material in response to compression. Since the layers are closely packed along the **a** direction, brucite is relatively stiff in this direction, and the **a**-axis compressibility reflects that of the O sublattice. The compressibility along **a** is largely constant with pressure. On the other hand, it is relatively easy to compress brucite along the **c** direction by pushing the layers together.

Neutron diffraction of brucite has been recently carried out to 11 GPa on normal samples (Catti et al., 1995) and to 9 GPa on deuterated samples (Parise et al., 1994). Above 5.4 GPa for $Mg(OD)_2$ and at 10.9 for $Mg(OH)_2$, improved fits were obtained for models in which the H or D atoms that move away from the threefold axis (Fig. 1) are split over three sites corresponding to the positions of the interlayer O atoms. Such models are consistent with the X-ray diffraction and spectroscopic data discussed above, although we observe evidence for H disorder at lower pressures in Raman experiments on $Mg(OH)_2$ than were obtained by neutron diffraction (Catti et al., 1995). This model also implies enhanced H bonding in the high-pressure phase, although the two studies differ regarding the pressure dependence of the O-H and O-D bond distances. In the $Mg(OD)_2$ study, the O-D bond distance increases from 0.95 Å at 1 bar to 1.03 Å at 9 GPa, whereas in the $Mg(OH)_2$ study, the O-H distance decreases from 0.96 Å at 1 bar to 0.91 Å at 11 GPa. The neutron diffraction studies confirm that most of the volume compression of brucite is due to a reduction in the interlayer spacing.

There is also evidence for long-range disordering of the H sublattice at ambient pressure in the divalent metal hydroxides $Ni(OH)_2$ (Greaves and Thomas, 1986) and $Ca(OH)_2$ (Desgranges et al., 1993). In $Ca(OH)_2$, the H atoms can be modeled as being dynamically disordered among three equivalent positions at 10° from the **c** axis at room temperature. At 180 K, there is evidence from neutron diffraction and thermodynamic data for a transition in which the H atoms become frozen at particular sites (Desgranges et al., 1993, 1994). A similar type of transition might be occurring in brucite at high pressure because of increased interlayer forces as the structure is compressed.

Comparison with Raman spectra of $Ca(OH)_2$

It is also of interest to compare the present results with Raman spectra for the isomorphous material $Ca(OH)_2$, which becomes X-ray amorphous at 11 GPa. For portlandite, there is a difference of a factor of three in the relative linear compressibilities. This is manifested as a change in the *c*/*a* ratio from 1.36 at ambient pressure to 1.29 at 10 GPa (Meade and Jeanloz, 1990). High-pressure Raman spectra for $Ca(OH)_2$ have also been recently measured (Meade et al., 1992; Duffy, in preparation). In portlandite, the lattice vibrations become extremely weak
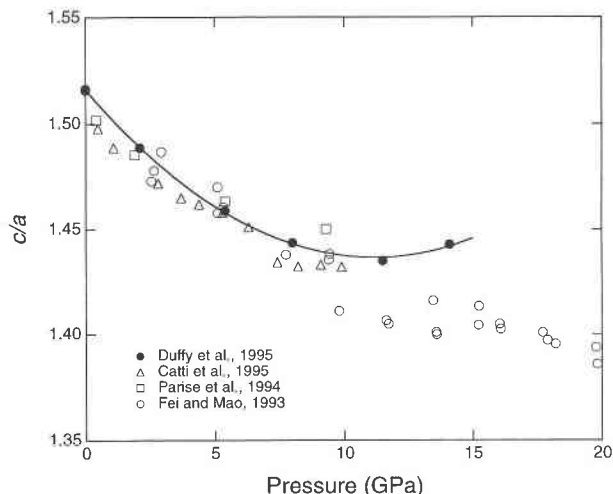

Fig. 8. Pressure dependence of the *c*/*a* ratio of brucite from X-ray and neutron diffraction experiments. Solid line is a fit to single-crystal data (Duffy et al., 1995).

and broad over a narrow pressure range around 12 GPa. This is consistent with X-ray diffraction and infrared spectroscopic data, which also show evidence for amorphization near this pressure (Meade and Jeanloz, 1990; Kruger et al., 1989).

For brucite, the O-H stretch frequency decreases linearly with pressure to at least 28 GPa. For portlandite, the stretch frequency is also red-shifted with pressure but decreases nonlinearly above 8 GPa, reflecting strong changes in the O-H bonding environment. The band width of the O-H stretch vibration broadens more strongly with pressure in $Ca(OH)_2$ than in $Mg(OH)_2$. At 10 GPa, the O-H band width in portlandite is more than five times larger than in brucite. These features are suggestive of more extensive disordering of the H positions in $Ca(OH)_2$. In portlandite, this disordering eventually extends to the Ca-O sublattice, as reflected in the loss of X-ray diffraction peaks near 11 GPa.

Hydrous minerals may have an important influence on the properties of the Earth's interior, even if present in relatively small amounts. A full understanding of the structure and stability of such phases requires very detailed characterization, including complete spectroscopic studies as well as X-ray diffraction. The former provide a powerful means of detecting small-scale changes that are not readily detectable by X-ray diffraction but that nevertheless have a significant bearing on the high-pressure behavior of the material.

REFERENCES CITED

Bernal, J.D., and Megaw, H.D. (1935) The function of hydrogen in intermolecular forces. Proceedings of the Royal Society of London, 151A, 384–420.

Bier, K.D., and Jodl, H.J. (1987) Tuning of the Fermi resonance of CO_2 and CS_2 by temperature, pressure, and matrix material. Journal of Chemical Physics, 86, 4406–4410.

Bowen, N.L., and Tuttle, O.F. (1949) The system $MgO-SiO_2-H_2O$. Geological Society of America Bulletin, 60, 439–460.

Catti, M., Ferraris, G., Hull, S., and Pavese, A. (1995) Static compression and H disorder in $Mg(OH)_2$ (brucite) to 11 GPa: A powder neutron diffraction study. Physics and Chemistry of Minerals, in press.

D'Arco, P., Causá, M., Roetti, C., and Silvi, B. (1993) Periodic Hartree-Fock study of a weakly bonded layer structure: Brucite, $Mg(OH)_2$. Physical Review B, 47, 3522–3529.

Dawson, P., Hadfield, C.D., and Wilkinson, G.R. (1973) The polarized infra-red and Raman spectra of $Mg(OH)_2$ and $Ca(OH)_2$. Journal of Physics and Chemistry of Solids, 34, 1217–1225.

Desgranges, L., Grebille, D., Calvarin, G., Chevrier, G., Floquet, N., Niepce, J.C. (1993) Hydrogen thermal motion in calcium hydroxide: $Ca(OH)_2$. Acta Crystallographica, B49, 812–817.

Desgranges, L., Grebille, D., Calvarin, G., Chhor, K., Pommier, C., Floquet, N., and Niepce, J.C. (1994) Structural and thermodynamic evidence of a change in thermal motion of hydrogen atoms in $Ca(OH)_2$ at low temperature. Journal of Physics and Chemistry of Solids, 55, 161–166.

Duffy, T.S., Ahrens, T.J., and Lange, M.A. (1991) The shock wave equation of state of brucite $Mg(OH)_2$. Journal of Geophysical Research, 96, 14319–14330.

Duffy, T.S., Fei, Y., Hemley, R.J., and Mao, H.K. (1993) A Raman spectroscopic study of a high-pressure phase transition in brucite. Eos, Spring Meeting Supplement, 169.

Duffy, T.S., Shu, J., Mao, H.K., and Hemley, R.J. (1995) Single-crystal X-ray diffraction of brucite to 14 GPa. Physics and Chemistry of Minerals, in press.

Elleman, D.D., and Williams, D. (1956) Proton positions in brucite crystals. Journal of Chemical Physics, 25, 742–744.

Fei, Y., and Mao, H.K. (1993) Static compression of $Mg(OH)_2$ to 78 GPa at high temperature and constraints on the equation of state of fluid H_2O. Journal of Geophysical Research, 98, 11875–11884.

Finger, L.W., and Prewitt, C.T. (1989) Predicted compositions for high-density hydrous magnesium silicates. Geophysical Research Letters, 16, 1395–1397.

Greaves, C., and Thomas, M.A. (1986) Refinement of the structure of deuterated nickel hydroxide, $Ni(OH)_2$, by powder neutron diffraction and evidence for structural disorder in samples with high surface area. Acta Crystallographica, B42, 51–55.

Hanson, R.C., and Jones, L.H. (1981) Infrared and Raman studies of pressure effects on the vibrational modes of solid CO_2. Journal of Chemical Physics, 75, 1102–1112.

Haycock, D.E., Kasrai, M., Nicholls, C.J., and Urch, D.S. (1978) The electronic structure of magnesium hydroxide (brucite) using x-ray emission, x-ray photoelectron, and Auger spectroscopy. Journal of the Chemical Society, Dalton Transactions, 1791–1796.

Hemley, R.J. (1987) Pressure dependence of Raman spectra of SiO_2 polymorphs: α-quartz, coesite, and stishovite. In M.H. Manghnani and Y. Syono, Eds., High-pressure research in mineral physics, p. 347–359. Terra Scientific, Tokyo.

Irving, A.J., Huang, W.-L., and Wyllie, P.J. (1977) Phase relations of portlandite, $Ca(OH)_2$ and brucite $Mg(OH)_2$ to 33 kilobars. American Journal of Science, 277, 313–321.

Johnson, M.C., and Walker, D. (1993) Brucite [$Mg(OH)_2$] dehydration and the molar volume of H_2O to 15 GPa. American Mineralogist, 78, 271–284.

Kanzaki, M. (1991) Stability of hydrous magnesium silicates in the mantle transition zone. Physics of the Earth and Planetary Interiors, 66, 307–312.

Kawai, N.T., Gibson, D.F.R., and Butler, I.S. (1990) Variable-temperature and -pressure spectroscopic studies of norbornadiene. Journal of Physical Chemistry, 94, 5729–5734.

Kennedy, G. (1956) The brucite-periclase equilibrium. American Journal of Science, 254, 567–573.

Kruger, M.B., Williams, Q., and Jeanloz, R. (1989) Vibrational spectra of $Mg(OH)_2$ and $Ca(OH)_2$ under pressure. Journal of Chemical Physics, 91, 5910–5915.

Leinenweber, K., Weidner, D.J., Vaughan, M., Wang, Y., and Zhang, J. (1993) MgO solubilities in H_2O above the brucite dehydration temperature. Eos, Spring Meeting Supplement, 170.

Lewis, S., and Sherman, W.F. (1979) Pressure-scanned Fermi resonance in the vibrational spectra of the sulphate ion. Spectrochimica Acta, 35A, 613–624.

Mao, H.K., Xu, J., and Bell, P.M. (1986) Calibration of the ruby pressure gauge to 800 kbar under quasi-hydrostatic conditions. Journal of Geophysical Research, 91, 4673–4676.

Meade, C., and Jeanloz, R. (1990) Static compression of $Ca(OH)_2$ at room temperature: Observations of amorphization and equation of state measurements to 10.7 GPa. Geophysical Research Letters, 17, 1157–1160.

Meade, C., Jeanloz, R., and Hemley, R.J. (1992) Spectroscopic and x-ray diffraction studies of metastable crystalline-amorphous transition in $Ca(OH)_2$ and serpentine. In Y. Syono and M.H. Manghnani, Eds., High-pressure research: Applications to Earth and planetary science, p. 485–492. Terra Scientific, Tokyo.

Mitra, S.S. (1962) Vibration spectra of solids. In F. Seitz and D. Turnbull, Eds., Solid state physics, vol. 13, p. 1–80. Academic, New York.

Nelmes, R.J., Loveday, J.S., Wilson, R.M., Besson, J.M., Pruzan, Ph., Klotz, S., Hamel, G., and Hull, S. (1993) Neutron diffraction study of the structure of deuterated ice VIII to 10 GPa. Physical Review Letters, 71, 1192–1195.

Olijnyk, H., Daufer, H., Jodl, H.-J. and Hochheimer, H.D. (1988) Effect of pressure and temperature on the Raman spectra of solid CO_2. Journal of Chemical Physics, 88, 4204–4212.

Parise, J.B., Leinenweber, K., Weidner, D.J., Tan, K., and Von Dreele, R.B. (1994) Pressure-induced H bonding: Neutron diffraction study of brucite, $Mg(OD)_2$, to 9.3 GPa. American Mineralogist, 79, 193–196.

Petch, H.E., and Megaw, H.D. (1954) Crystal structure of brucite $Mg(OH)_2$ and portlandite $Ca(OH)_2$ in relation to infrared absorption. Journal of the Optical Society of America, 44, 744–745.

Redfern, S.A.T., and Wood, B.J. (1992) Thermal expression of brucite, $Mg(OH)_2$. American Mineralogist, 77, 1129–1132.

Sherman, D.M. (1991) Hartree-Fock band structure, equation of state, and pressure-induced hydrogen bonding in brucite, $Mg(OH)_2$. American Mineralogist, 76, 1769–1772.

Shimizu, H. (1985) Pressure-tuning resonance between the vibron and the libron in CH_2Br_2 and CD_2Br_2 molecular solids. Physical Review B, 32, 4120–4125.

Simakov, G.V., Pavlovskiy, M.N., Kalashnikov, N.G., and Trunin, R.F. (1974) Shock compressibility of twelve minerals. Izvestia Solid Earth Physics, 10, 11–17.

Sushchinskii, M.M. (1972) Raman spectra of molecules and crystals, 446 p. Keter, New York.

Zigan, F., and Rothbauer, R. (1967) Neutronenbeugungsmessungen am Brucit. Neues Jahrbuch für Mineralogie Monatshefte, 137–143.